Bulgarian Chemical Communications, Volume 57, Issue 4 (pp. 331-338) 2025 DOI: 10.34049/bcc.57.4.5678

Phytonano synthesis of MgO nanoparticles using aqueous leaf extract of *Hibiscus rosa sinensis*: comprehensive characterization and assessment of their antibacterial and anti-oncogenic activities

G.K. Prashanth[1,2*], H.S. Lalithamba[3], S. Rao[4], N.P. Bhagya[5], K.V. Rashmi[6], H. N. Akolkar[7]

[1]*Research and Development Center, Department of Chemistry, Sir M. Visvesvaraya Institute of Technology, Bengaluru-562 157, India*
[2]*Visvesvaraya Technological University, Belagavi-590 018, India*
[3]*Department of Chemistry, Siddaganga Institute of Technology, Tumkur-572 103, India*
[4]*Department of Chemistry, Nitte Meenakshi Institute of Technology, Nitte (Deemed to be University), Bengaluru-560 064, India*
[5]*Department of Chemistry, Sai Vidya Institute of Technology, Bengaluru-560 064, India*
[6]*Department of Bio-Technology, Sir M. Visvesvaraya Institute of Technology, Bengaluru-562 157, India*
[7]*Department of Chemistry, Abasaheb Marathe Arts, and New Commerce, Science College, Ratnagiri-415 612, India*

Received: November 03, 2024; Revised: October 06, 2025

In the realm of nanostructured materials and nanotechnology, MgO nanoparticles (MgO-NPs) have garnered significant attention due to their unique properties and myriad applications. This work explores the synthesis of MgO-NPs *via* green chemistry principles, utilizing a sustainable approach with *Hibiscus rosa sinensis* leaf extract through the solution combustion synthesis technique. Characterization using PXRD confirmed a cubic crystal structure with an average crystallite size of ~25 nm, while SEM revealed porous morphology and BET analysis showed a surface area of 32.76 m^2/g. The antibacterial activity demonstrated strong inhibition against *E. coli* and *S. aureus*, with minimum inhibitory concentration (MIC) values of 15.62 µg/mL and 31.25 µg/mL, respectively, and maximum zones of inhibition of 14.5 mm and 19.5 mm. Anti-oncogenic evaluation against MDA-MB-231 and HeLa cell lines revealed dose-dependent cytotoxicity with an IC50 value of 378.7 µg/mL. Blood hemolysis testing confirmed <5% hemolysis up to 10 mg/mL, affirming the biocompatibility of the synthesized MgO-NPs. These results underscore the potential of MgO-NPs as eco-friendly antibacterial and anticancer agents.

Keywords: MgO-NPs; Solution combustion; Green fuel; Antibacterial; MTT assay; Blood hemolysis

INTRODUCTION

In recent decades, there has been significant interest in nanostructured materials and nanotechnology as they intersect within the techno-economic sphere [1]. This heightened attention arises primarily from the potential of reducing materials to the nanoscale, which can result in distinctive properties not achievable in bulk materials at larger scales [2]. MgO-NPs stand out among essential metal oxide nanoparticles due to their biocompatibility, exceptional stability, cost-effectiveness, high ionic properties, crystal structure, and effectiveness as safe and efficient contaminant adsorbents [3, 4]. Over the past two decades, the myriad applications and distinctive characteristics of MgO-NPs have garnered significant attention from researchers worldwide, surpassing interest in other metal oxide nanoparticles [5-8]. They are economically viable, highly biocompatible, and stable under extreme conditions [9].

MgO-NPs possess a unique set of properties that make them highly effective across diverse applications. They are cost-effective, biocompatible, and remain stable even under extreme conditions [10–12]. Owing to their strong adsorption capability, MgO-NPs serve as efficient and safe adsorbents for a range of contaminants [13,14]. Their wide band gap, exceptional thermodynamic stability, low dielectric constant, and low refractive index further support their use in catalysis, ceramics, toxic-waste remediation, and as functional additives in diesel engines, paints, and superconducting materials [15–20]. Beyond these industrial roles, MgO-NPs also show notable biomedical potential as antibacterial [21] and anti-oncogenic agents [22]. Their antibacterial action is attributed to multiple mechanisms, including protein denaturation, DNA damage, disruption of cell membranes and enzymes, interference with transmembrane electron transport, and damage to cellular storage granules [23, 24].

* To whom all correspondence should be sent:
E-mail: *prashanth_chem@sirmvit.edu*

The green synthesis method for NPs aligns with the twelve principles of green chemistry. This involves designing and creating nanoparticles using non-toxic chemicals, renewable materials, environmentally friendly solvents, and generating degradable waste products [25]. From a green chemistry perspective, three critical stages in NPs preparation include utilizing benign solvent media, non-toxic reducing agents, and environmentally safe stabilization agents [26]. Additionally, selecting an appropriate capping agent to passivate the NPs surface is another crucial factor [27]. Currently, the production of nanoscale metals predominantly relies on chemical processes, leading to unintended consequences such as environmental contamination, high energy usage, and potential health risks. To address these issues, a sustainable approach known as green synthesis has emerged, utilizing plant extracts in lieu of conventional industrial chemicals to reduce metal ions. Green synthesis offers advantages over traditional methods, including lower costs, reduced pollution, and enhanced safety for both the environment and human health.

The solution combustion synthesis technique stands out as a versatile approach for producing NPs applicable across various fields. Its adaptability is evident in its ability to generate numerous compounds, particularly oxides, making it a cornerstone technique in materials science. Its effectiveness lies in its straightforward implementation, high throughput, diverse chemical capabilities, and ability to create powders with high surface areas.

Based on the provided background, we propose a straightforward method for producing a versatile oxide material, MgO nanoparticles (NPs), possessing various desirable properties such as a wide band gap, exceptional thermodynamic stability, low dielectric constant, and a low refractive index. These properties render them suitable for a wide range of applications including catalysis, ceramics, toxic waste remediation, antibacterial agents, and as additives in refractory, paint, and superconductor products. We utilized a green synthesis approach employing aqueous leaf extract of hibiscus through the SCS method. The resulting nanoparticles underwent characterization through techniques such as PXRD, SEM, and BET surface area analysis. Furthermore, we evaluated the antibacterial activity of the nanoparticles against *S. aureus* and *E. coli,* determining their MIC values. Additionally, we assessed their anti-oncogenic activity using the MTT assay against MDA-MB-231 and HeLa cell lines, while their biocompatibility was evaluated through blood hemolysis testing.

MATERIALS AND METHODS

Chemicals and reagents

Magnesium nitrate hexahydrate [$Mg(NO_3)_2.6H_2O$, AR 99% Himedia], citric acid [$C_6H_8O_7$, AR, 99 %, SD Fine], nutrient agar [Himedia], potato dextrose agar [Himedia], Dulbecco's modified eagle's medium [DMEM, Gibco], dimethyl sulfoxide [C_2H_6SO, AR 99% Merck], MTT [$C_{18}H_{16}BrN_5S$, 97.5%, Sigma-Aldrich] were procured commercially and hibiscus leaves were plucked from Sir MVIT campus, Bengaluru. The cell lines used for cytotoxicity testing were procured from the ATCC.

Aqueous leaf extract and its phytochemical screening

The process began with cleansing of the leaves using water, followed by a 15-day period of air drying. Subsequently, a solution of hibiscus leaf extract was prepared through Soxhlet extraction over 72 h, utilizing 10 g of leaves in 150 mL of double distilled water.

Combustion synthesis of MgO-NPs

To synthesize MgO-NPs, the appropriate quantity of $Mg(NO_3)_2 \cdot 6H_2O$, was dissolved in 5 mL of plant extract, followed by the addition of 10 mL of distilled water. The resulting mixture was transferred to a crystallizing dish and placed into a preheated muffle furnace set at 500 ± 10 °C. Within 5 min, a visible flame emerged, indicating the initiation of an exothermic reaction between the phytochemicals present in the plant extract and the magnesium ions, leading to the formation of MgO-NPs.

Characterization

Various techniques were employed to characterize the synthesized MgO-NPs. PXRD analysis was conducted using a PANalytical X'pert diffractometer with Cu Kα radiation (λ = 1.541 Å) operating at 50 kV voltage and 30 mA current, covering a 2θ range from 20° to 80° to investigate phase purity and crystalline structure. Surface morphology and composition were examined using JEOL Model JSM - 6390LV with an EDS system (OXFORD XMX N). Surface area measurements using the BET method were conducted utilizing Quantachrome ASiQwin.

Evaluating the biological potential of green-synthesized MgO-NPs

- *Antibacterial activity.* The antibacterial activity of MgO NPs was carried out by the well diffusion method in MH agar media as followed in our previous work [28]. The bacteria (*E. coli*, and *S. aureus*) were cultured overnight at 37 °C in MH and adjusted to a final density of 107 CFU/mL by 0.5 McFarland standards. About 25 mL of molten MH agar was poured into sterile petri plates. The plates were allowed to solidify, after which 100 µL of the pathogenic bacteria cultures were transferred onto plate and made culture lawn by using sterile L-rod spreader. Homogeneous dispersions of MgO-NPs with different concentrations ranging from 1000-250 µg/mL (with two-fold dilution) were prepared by ultrasonication. Wells were cut and dispersions of MgO NPs (of different concentrations) were loaded. The plates were incubated at 37 °C for 24 h. The antibacterial activity was determined by measuring the diameter of the ZOI formed around the wells. Bacterial cultures grown in tryptic soy broth (adjusted to 1-2 × 10^5 cells/mL) were utilized for inoculation. Aqueous dispersions of MgO-NPs ranging from 1000 to 1.953 µg/mL (two-fold dilutions) in MH broth were tested against these cultures. RPMI media (MH broth) with and without MgO NPs served as controls. In 96-well plates, 90 µL of test sample dispersions at different concentrations were mixed with 10 µL of inoculum in triplicate. Control wells contained 90 µL of RPMI media (MH agar) without the drug mixed with 10 µL of inoculum. Treated bacterial cultures were incubated at 35°C. After 24-48 h, the plates were observed, and optical density was measured at 600 nm using a Tecan plate reader.

Percent inhibition was calculated using the formula: [absorbance control (untreated) - absorbance (treated)] / absorbance control. The MIC was determined as the lowest concentration of MgO-NPs that resulted in at least 50% inhibition of OD compared to the control.

- *Anti-oncogenic activity.* The anti-oncogenic potential of MgO-NPs was evaluated using the MTT assay, as described in our previous research with slight modifications [28-33]. MDA-MB-231 and HeLa cell lines were trypsinized when they reached 80% confluency. A total of 15,000 viable cells/well were seeded in a 96-well plate and incubated for 24 h at 37°C in a 5% CO_2 incubator. MgO-NPs ranging from 0 to 320 µg/mL in DMEM without 10% fetal bovine serum were added and incubated for 24 h. Following NPs treatment, the media were removed, and 200 µL/well of a 10% MTT working solution was added and incubated for another 24 h. Afterward, the media were aspirated, and 200 µL of a medium containing 10% MTT reagent was added to each well, resulting in a final concentration of 0.5 mg/mL. The plate was then incubated at 37°C in a 5% CO_2 atmosphere for 3 h. After incubation, the culture medium was removed without disturbing the formed crystals, and 100 µL of solubilization solution (DMSO) was added to each well. The plate was gently shaken on a gyratory shaker to dissolve the formazan crystals, and the absorbance was measured at 630 nm using a microplate reader. The percentage of growth inhibition was calculated after subtracting the background and blank values, and the concentration of the test drug required to inhibit cell growth by 50% (IC50) was determined from the dose-response curve for each cell line. Camptothecin was used as the standard drug, with IC50 values of 75 µM and 50 µM for MDA-MB-231 and HeLa cell lines, respectively.

- *Evaluation of cytotoxicity through blood hemolysis.* The hemolysis activity test for MgO NPs followed the protocol outlined by Das *et al*. (2013) [34]. Briefly, 9 mL of sheep blood was mixed with 1 mL of 3.8% sodium citrate to prevent blood coagulation. The mixture was centrifuged at 3000 rpm for 5 min to remove platelet-rich plasma. The remaining RBC pellet was suspended in 10 mL of PBS at pH 7.4 to create a uniform cell suspension. MgO-NPs at concentrations ranging from 0.25 to 10.0 mg/mL were prepared in separate test tubes. To each test tube, 2 mL of erythrocyte suspension was added, and the tubes were inverted and gently shaken to ensure contact between the blood and MgO NPs. The tubes were then incubated at 37°C for 90 min. After incubation, the samples were centrifuged at 3000 rpm for 5 min to pellet the RBCs. The supernatant was collected, and its absorbance was measured at 540 nm using a UV-visible spectrophotometer against a blank PBS solution.

RESULTS AND DISCUSSION

Crystal structure, surface morphology and BET surface area

PXRD pattern of MgO-NPs is presented in Fig. 1. The diffraction peaks observed at 2θ angles of 37.76°, 43.12°, 64.97°, 74.45°, and 78.12° were found to correspond to the crystallographic planes (111), (200), (220), (311), and (222), respectively, within the face-centered cubic (FCC) lattice of magnesium. These findings strongly supported the crystalline nature of MgO-NPs. The obtained diffraction pattern aligned closely with the established diffraction data for MgO-NPs (JCPDS file No. 89-4248). By applying the Scherrer equation

to the diffraction peaks, the average crystallite size was determined to be ≈ 25 nm.

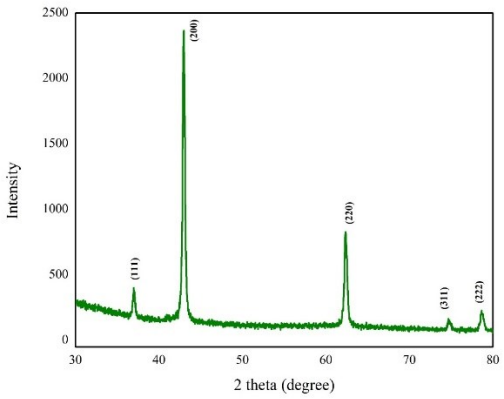

Figure 1. PXRD pattern of MgO NPs

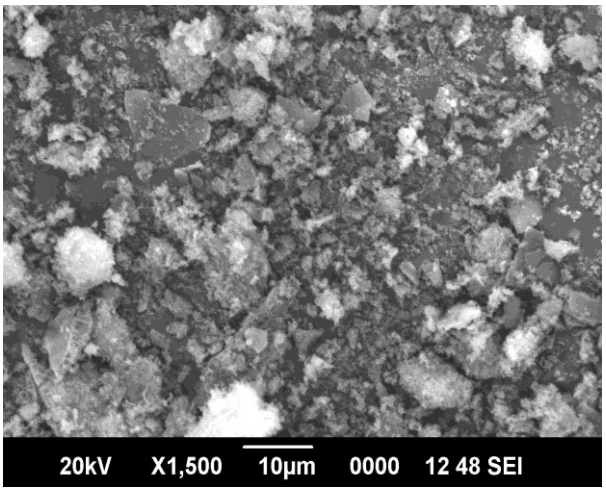

Figure 2. SEM image of MgO NPs

The SEM findings (Fig. 2) indicate that the MgO-NPs appear to exhibit porosity and significant agglomeration with nanoentities. Consequently, the accurate determination of MgO particle size from the current SEM results is challenging.

Results of surface area measurements indicated a BET surface area of 32.762 m^2/g.

Biological potential of MgO-NPs

- *Antibacterial activity.* The observed ZOI of MgO-NPs against *E. coli* and *S. aureus*, along with the MIC values, are summarized in Table 1 and depicted in Figure 3. The results clearly demonstrate that MgO-NPs possess significant antibacterial activity against both Gram-negative and Gram-positive strains, with inhibition zones increasing in a concentration-dependent manner. For *E. coli*, the maximum ZOI reached 14.5 mm at 1000 µg/mL with an MIC of 15.62 µg/mL, while for *S. aureus*, a maximum ZOI of 19.5 mm was observed at the same concentration, with an MIC of 31.25 µg/mL. These results highlight the broad-spectrum antibacterial efficacy of MgO-NPs.

The difference in sensitivity between the two bacterial strains can be correlated to their structural features. Gram-negative *E. coli*, with its thinner peptidoglycan layer and outer lipid membrane, exhibited greater susceptibility at lower concentrations, whereas Gram-positive *S. aureus*, despite its thicker cell wall, showed strong inhibition at higher concentrations. The antibacterial effect of MgO-NPs may be attributed to multiple mechanisms acting simultaneously. One possible mechanism is the generation of reactive oxygen species (ROS) on the surface of MgO-NPs, which induces oxidative stress in bacterial cells. In addition, Mg^{2+} ions released from the nanoparticles can penetrate bacterial cells, disrupting enzymatic activities and impairing metabolic processes. The direct interaction of MgO-NPs with the bacterial cell membrane may also lead to increased permeability, leakage of intracellular components, and eventual cell lysis.

Table 1. Results of antibacterial activity of MgO NPs and standard antibiotic (ZOI in mm)

Pathogen	Conc. (µg/mL)	ZOI Mean ± SD (mm)		MIC (µg/mL)
		MgO-NPs	Positive control (Ofloxacin 100 µg/mL)	
E. coli	125	0.00 ± 0.00	40.77 ± 1.05	15.62
	250	7.00 ± 0.00		
	500	8.50 ± 0.00		
	1000	14.50 ± 0.816		
S. aureus	125	0.00 ± 0.00	38.0 ± 1.06	31.25
	250	0.00 ± 0.00		
	500	0.00 ± 0.00		
	1000	19.50 ± 0.577		

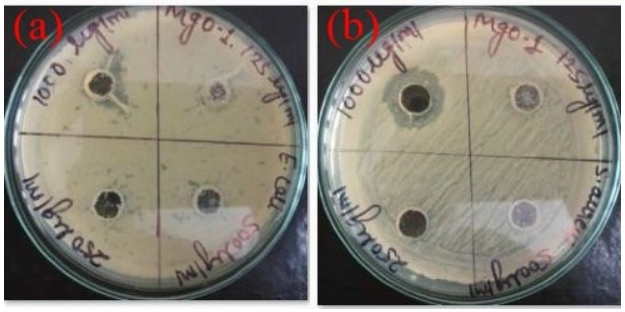

Figure 3. ZOI against (a) *E. coli*, and (b) *S. aureus*

Taken together, these findings confirm that the biosynthesized MgO-NPs are highly effective antibacterial agents, acting through a combination of ROS generation, ion release, and membrane disruption mechanisms, as illustrated in Figure 4 [35].

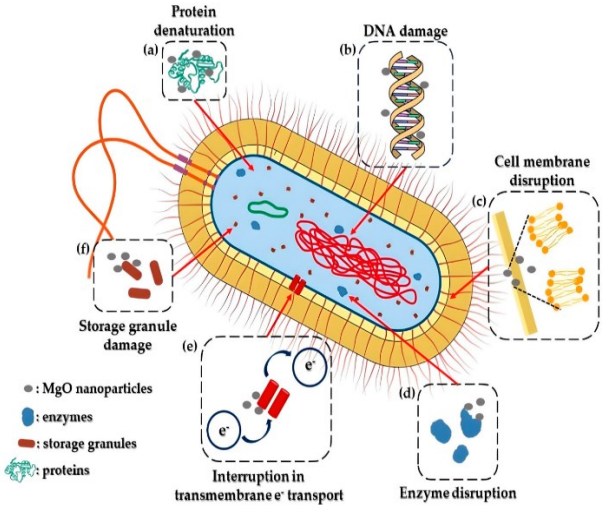

Figure 4. Probable mechanism of antibacterial activity of MgO-NPs [20]

- *Anti-oncogenic activity.* The effect of MgO-NPs on the viability of MDA-MB-231 and HeLa cells was investigated using the MTT assay, and the results are presented in Figure 5. A concentration-dependent reduction in cell viability was observed, with higher nanoparticle concentrations leading to greater cytotoxic effects. The IC50 value for MgO-NPs was determined to be 378.7 µg/mL (Figure 6), confirming moderate anticancer potential. Optical microscopy images (Figure 8) further illustrate the progressive morphological changes in cancer cells, including shrinkage, membrane blebbing, and loss of adherence with increasing nanoparticle concentration, in comparison to untreated controls.

The anticancer activity of MgO-NPs can be attributed to multiple factors. The generation of reactive oxygen species (ROS) within the cellular environment may induce oxidative stress, leading to DNA damage, mitochondrial dysfunction, and apoptosis. Additionally, the release of Mg^{2+} ions could interfere with intracellular signaling pathways, contributing to reduced proliferation. The direct interaction of MgO-NPs with the cancer cell membrane may further destabilize its integrity, triggering cell death. The plausible mechanism of action is schematically illustrated in Figure 7. Collectively, these findings suggest that MgO-NPs exhibit promising anticancer properties, mediated through ROS generation, ion release, and induction of apoptosis in cancer cells.

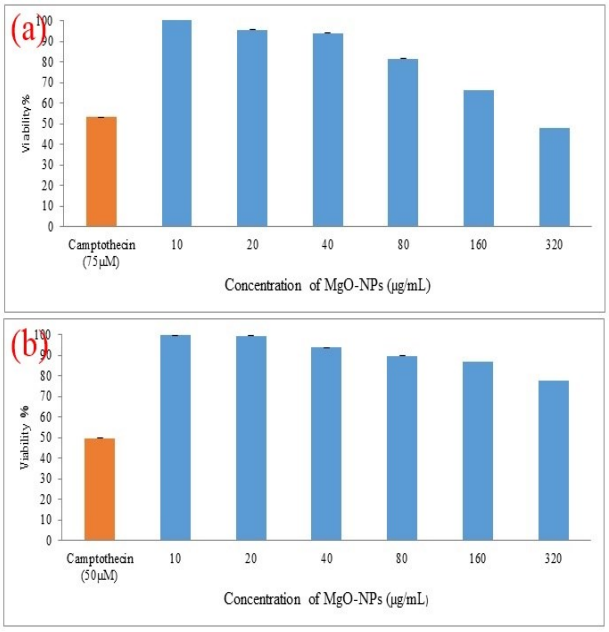

Figure 5. Cell viability of (a) MDA-MB-231, and (b) HeLa by the action of MgO-NPs

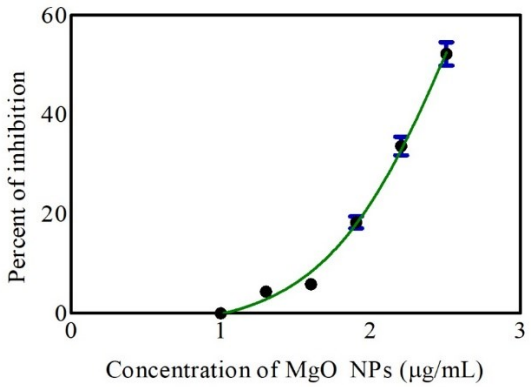

Figure 6. IC50 determination of MgO-NPs in MDA-MB-231 cell line

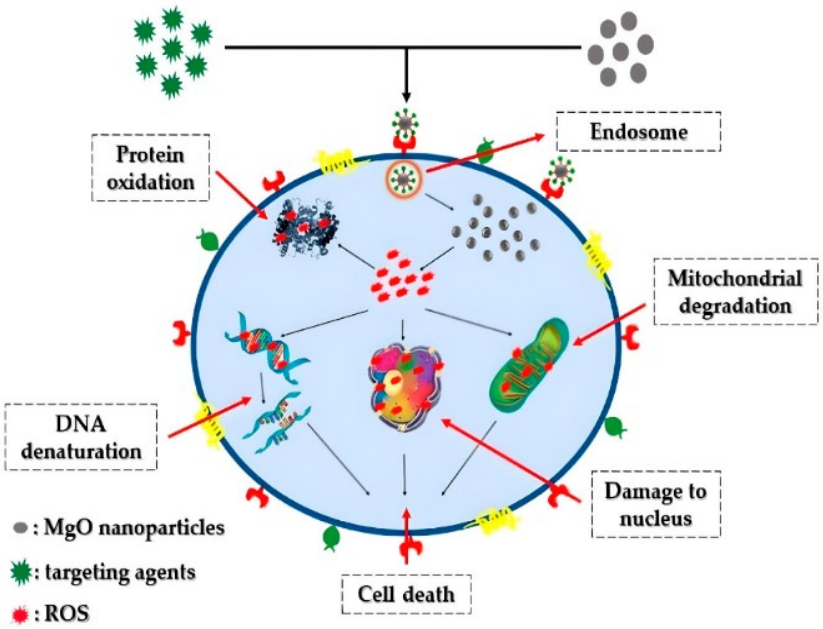

Figure 7. Probable anti-oncogenic mechanism of MgO-NPs [35]

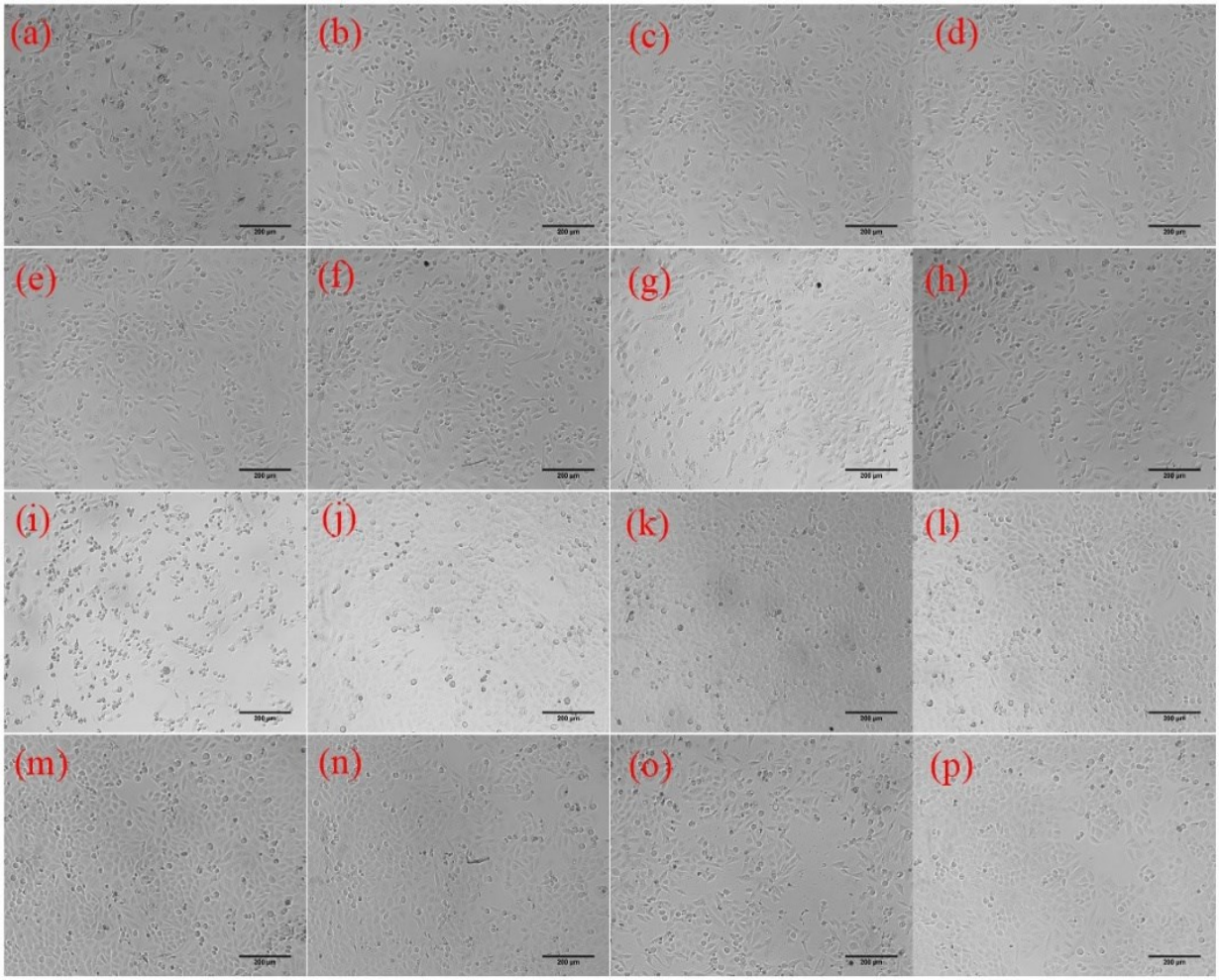

Figure 8. MDA-MB-231 treated with (a) Camptothecin 50 µM, (b) 10 µg/mL, (c) 20 µg/mL, (d) 40 µg/mL, (e) 80 µg/mL, (f) 160 µg/mL, (g) 320 µg/mL of MgO-NPs, (h) Untreated; HeLa treated with (i) Camptothecin 50 µM, (j) 10 µg/mL, (k) 20 µg/mL, (l) 40 µg/mL, (m) 80 µg/mL, (n) 160 µg/mL, (o) 320 µg/mL of MgO-NPs, and (p) Untreated

- *Blood hemolysis.* The cytocompatibility of MgO-NPs was further assessed by hemolysis assays using sheep erythrocytes. The results, presented in Table 2, demonstrate that hemolysis percentages remained below 5% even at the highest tested concentration of 10 mg/mL. This indicates that the synthesized MgO-NPs exhibit good hemocompatibility and are unlikely to cause significant damage to red blood cells.

The low hemolytic activity suggests that the surface characteristics of the MgO-NPs, including their phytochemical capping from *Hibiscus rosa sinensis* extract, may help minimize adverse interactions with erythrocyte membranes. A hemolysis percentage below 5% is widely considered as the threshold for blood compatibility, implying that the concentrations used in antibacterial and anticancer studies fall well within the biocompatible range. The minimal disruption of erythrocyte membranes observed in this study supports the safe application of MgO-NPs in biomedical contexts, particularly in antibacterial and anticancer therapies where systemic exposure is a consideration.

Table 2. Blood hemolysis by MgO-NPs

S. No.	Concentration of MgO-NPs (/mL)	Hemolytic activity (%)
1	0.25 mg	0.57
2	0.5 mg	1.06
3	1 mg	1.30
4	2.5 mg	2.19
5	5 mg	3.08
6	10 mg	4.63

CONCLUSION

This study successfully illustrates the synthesis of MgO-NPs *via* SCS, utilizing hibiscus leaf extract as a bio-fuel. Analysis through PXRD revealed the cubic crystal structure of MgO, with an average crystallite size of 25 nm. SEM image displayed the spherical morphology of the particles, albeit with uneven sizes, while BET results indicated a surface area of 32.762 m^2/g. Antibacterial assessments demonstrated the efficacy of MgO against both Gram-negative *E. coli* and Gram-positive *S. aureus*, with MIC values of 15.62 µg/mL and 31.25 µg/mL, respectively. Further, MTT assay results unveiled moderate anti-oncogenic activity of MgO-NPs, with an IC50 value of 378.7 µg/mL. Furthermore, blood hemolysis testing affirmed the biocompatibility of MgO-NPs up to a concentration of 10 mg/mL.

Abbreviations

MgO: Magnesium oxide
NPs: Nanoparticles
SCS: Solution combustion synthesis
PXRD: Powder-X-ray diffraction
SEM: Scanning electron microscopy
BET: Brunauer–Emmett–Teller
MH: Mueller–Hinton
RPMI: Roswell Park Memorial Institute
MTT: (3-[4,5-dimethylthiazol-2-yl]-2,5-diphenyl tetrazolium bromide)
ATCC: American Type Culture Collection
ZOI: zone of inhibition
RBC: Red blood cells
PBS: Phosphate-buffered saline
E. coli: *Escherichia coli*
S. aureus: *Staphylococcus aureus*

Declarations

Funding: The authors declare that no specific grant was received from funding agencies in the public, commercial, or not-for-profit sectors for this work.
Conflict of interest: The authors declare no conflict of interest.
Ethical approval: Not required.
Consent to participate: Not applicable.
Consent for publication: All authors have read and approved the final manuscript and consent to its publication.
Availability of Data and Materials: All data generated or analyzed during this study are included in this article.
Authors' contributions: G.K. Prashanth: Conceptualization, methodology, supervision, writing—review & editing; **Srilatha Rao:** Data curation, formal analysis, writing—original draft;

- **H.S. Lalithamba:** Characterization studies, validation; **K.V. Rashmi:** Cytotoxicity and hemolysis assays, Biological assays, data interpretation; **N.P. Bhagya** and **H. K. N. Akolkar:** Literature review, writing—review & editing.

REFERENCES

1. F. Trotta, A. Mele, Nanosponges, John Wiley & Sons, Ltd., Hoboken, NJ, USA, 2019, p. 142.
2. S.B. Mitra, Chapter 2-Nanoparticles for dental materials: Synthesis, analysis, and applications, in: K. Subramani, W. Ahmed (eds.), Emerging Nanotechnologies in Dentistry, 2nd edn., William Andrew Publishing, Norwich, NY, USA, 2018, p, 17.
3. F. Mahmoudi, F. Mahmoudi, K.H. Gollo, M.M. Amini, *Biol. Trace Elem. Res.,* **199,** 1967 (2021).
4. A.A.A.A. Alrashed, O.A. Akbari, A. Heydari, D. Toghraie, M. Zarringhalam, G.A.S. Shabani, A.R. Seifi, M. Goodarzi, *Phys. B Condens. Matter,* **537,** 176 (2018).

5. M.A. Amin, A.M. Abu-Elsaoud, A.I. Nowwar, A.T. Abdelwahab, M.A. Awad, S.E.D. Hassan, F. Boufahja, A. Fouda, A. Elkelish, *Green Process. Synth.,* **13** (1), 20230215 (2024).
6. S. Abinaya, H.P. Kavitha, *ACS Omega,* **8** (6) 5225 (2023).
7. Z. Abbas, M.A. Hassan, W. Huang, H. Yu, M. Xu, X. Chang, X. Fang, L. Liu, *Agronomy,* **14** (3), 617 (2024).
8. S.M. Shaikh, P.V. Desai, *Indian J. Exp. Biol.,* **62** (4), 229 (2024).
9. S. Faisal, J. Abdullah, S.A. Shah, S. Shah, M. Rizwan, N. Zaman, Z. Hussain, M.N. Uddin, N. Bibi, A. Khattak, *Catalysts,* **11** (7), 780 (2021).
10. N., Thakur, J., Ghosh, S.K., Pandey, A. Pabbathi, J., Das, *Inorganic Chemistry Communications*, **146**, 110156 (2022).
11. A. Muhaymin, H.E.A. Mohamed, K. Hkiri, A. Safdar, S. Azizi, M. Maaza, *Scientific Reports*, **14**(1), 20135 (2024).
12. I. Humaira Ahmad, H.A. Shakir, M. Khan, S. Ali, M. Alshahrani, M. Franco, M. Irfan, *ChemBioEng Reviews*, **11**(3), 447 (2024).
13. H.C.S. Perera, V. Gurunanthanan, A. Singh, M.M.M.G.P.G. Mantilaka, G. Das, S. Arya, *Journal of Magnesium and Alloys*, **12**(5), 1709 (2024).
14. Kuruthukulangara, Nethra, I. V. Asharani, *Journal of Cluster Science,* **35** (8), 2681 (2024).
15. K. Tharani, A.J. Christy, S. Sagadevan, L.C. Nehru, *Chemical Physics Letters*, **763**, 138216 (2021).
16. B. Debnath, S. Das, S. Debnath, M. Debbarma, S. Chattopadhyaya, *Computational Condensed Matter*, **41**, e00959 (2024).
17. S. Rani, P. Kumar, N. Kataria, *Journal of the Taiwan Institute of Chemical Engineers*, **166**, 105566. 2025.
18. S.B. Arun, K.V. Yatish, G. Tigari, G.K. Prashanth, H.S. Lalithamba, K. Pramoda, *Renewable Energy*, 124218 (2025).
19. H. Tang, S. Li, Y. Zhang, Y. Na, C. Sun, D. Zhao, J. Liu, Z. Zhou, *Journal of Cleaner Production*, **380**, 135035 (2022).
20. F. Yu, Y. Xue, C. Zhong, J. Song, Q. Nie, X. Hou, B. Wang, *Micromachines*, **14**(10), 1914 (2023).
21. X. Li, H. Liu, Y. He, Z. Li, F. Y. Zhan, Li, J. Zhao, *Ceramics International*, **50**(21), 42877 (2024).
22. P. Arthi, K. Hema, S.V.G. Rani, R. Sugarthi, A. Sivapunniyam, T. Perumal, P.K. Seetharaman, K.R. Ramalingam, C. Jayashree, *Journal of Inorganic and Organometallic Polymers and Materials*, 1 (2025).
23. M. Ramezani Farani, M. Farsadrooh, I. Zare, A. Gholami, O. Akhavan, *Catalysts*, **13**(4), 642 (2023).
24. M.A. Gatou, E. Skylla, P. Dourou, N. Pippa, M. Gazouli, N. Lagopati, E.A. Pavlatou, *Crystals*, **14**(3), 215 (2024).
25. J. Virkutyte, R.S. Varma, *Chem. Sci.,* **2** 837 (2011).
26. P. Raveendran, J. Fu, S.L. Wallen, *J. Am. Chem. Soc.,* **125,** 13940 (2003).
27. A. Annu, A. Ali, S. Ahmed, *Nanomedicine,* 1 (2018).
28. K.R. Mohana, P.A. Prashanth, B.M. Nagabhushana, G.M. Krishnaiah, H.G. Nagendra, M.S. Dileep, G.K. Prashanth, *Int. J. Adv. Sci. Technol.,* **29** (8s), 3668 (2020).
29. G.K. Prashanth, H.M. Sathyananda, P.A. Prashanth, M. Gadewar, M. Mutthuraju, S.B. Prabhu, B.M. Nagabhushana, C. Shivakumara, S. Rao, D. Mohanty, *Appl. Phys. A,* **128** (7) 614 (2022).
30. S. Nagarajaiah, A. Shivanna Giresha, P. Gopala Krishna, M. Manikrao Gadewar, M. Praveen, N. Nanda, D. Urs, K. Krishnappa Dharmappa, B. Mutta Nagabhushana, S. Rao, M. Mahadeva Swamy, *Chem. Biodivers.,* e202301533 (2024).
31. S. Nagarajaiah, N. Nanda, P. Manjappa, B.M. Nagabhushana, M. Gadewar, S. Rao, P.G. Krishna, *Appl. Phys. A,* **129** (6), 461 (2023).
32. P.G. Krishna, P.P. Ananthaswamy, T. Yadavalli, N.B. Mutta, A. Sannaiah, Y. Shivanna, *Mater. Sci. Eng. C,* **62,** 919 (2016).
33. P.G. Krishna, P. Ananthaswamy, P. Trivedi, V. Chaturvedi, N.B. Mutta, A. Sannaiah, A. Erra, T. Yadavalli, *Mater. Sci. Eng. C,* **75,** 1026 (2017).
34. D. Das, B.C. Nath, P. Phukon, A. Kalita, S.K. Dolui, *Colloids Surf. B: Biointerfaces,* **111,** 556 (2013).
35. M.A. Gatou, E. Skylla, P. Dourou, N. Pippa, M. Gazouli, N. Lagopati, E.A. Pavlatou, *Crystals,* **14** (3), 215 (2024).